Characteristics of Millimeter-Wave Radiation in a Corrugated Ferrite Slab Structure

SIDICK ERKIN, NION SOCK CHANG, MEMBER, IEEE, HESHMATOLLAH MAHERI, AND MAKOTO TSUTSUMI, MEMBER, IEEE

Abstract—**The characteristics of millimeter-wave radiation in a corrugated ferrite slab supported by a grounded dielectric slab are investigated both theoretically and experimentally. Theoretical analysis is performed by the perturbation theory combined with multiple space scales for the transverse electric mode. A pair of amplitude transport equations are derived, and the characteristics of the leaky wave are explained in terms of the radiation angle and the radiation efficiency. Experiments are carried out by using the layered structure composed of a corrugated polycrystalline yttrium iron garnet slab and a Teflon slab in the frequency range from 40 to 50 GHz. The experimental results are compared with the theory.**

I. Introduction

LEAKY WAVE PHENOMENA in corrugated waveguides find applications in high-resolution radar at millimeter waves and in grating couplers in integrated optics [1]. Recently the authors have studied experimentally the radiation characteristics of millimeter waves in a layered corrugated ferrite slab structure, and observed the magnetically scannable behavior of the leaky waves [2], [3]. However, rigorous analysis of the leaky waves on a corrugated ferrite structure has not yet been carried out. On the other hand, a perturbation method combined with multiple space scales has been used recently to analyze the leaky wave phenomena in corrugated dielectric waveguides [4]–[6]. This method has the advantage of predicting not only the radiation angle but also the radiation efficiency.

This paper presents an analysis of the leaky wave in a corrugated ferrite dielectric slab structure, which may be useful for the practical design of millimeter-wave antenna. The perturbation method combined with multiple space scales is used, and two amplitude transport equations characterizing the coupling between the guided wave and the incident and radiated waves are systematically derived. The radiation efficiency is determined from the characteristics of the transmitting antenna. The main beam direction and the radiation efficiency are numerically evaluated as a function of the bias magnetic field for two different operating frequencies, and the theoretical results are confirmed in experiments carried out in the millimeter-wave frequency.

Manuscript received May 11, 1987; revised October 5, 1987.

S. Erkin and N. S. Chang are with the Department of Communication Engineering, Faculty of Engineering, Osaka Electro-Communication University, 18-8 Hatsu-cho, Neyagawa, Osaka 572, Japan.

H. Maheri and M. Tsutsumi are with the Department of Communication Engineering, Faculty of Engineering, Osaka University, Yamadaoka, Suita, Osaka 565, Japan.

IEEE Log Number 8718871.

II. Theory

A. Formulation of the Problem

The geometry of the corrugated ferrite slab structure is shown in Fig. 1. The weak sinusoidal corrugation represented by the function $x = h(y)$ is located on a surface of the ferrite slab, which has the permeability tensor $\tilde{\mu}$. The ferrite slab is supported by another grounded dielectric slab with relative permittivity ϵ_d and is magnetized in the z direction. The thicknesses of the ferrite and dielectric slabs are h and d, respectively. A major part of electromagnetic energy in the structure of Fig. 1 is concentrated within the ferrite slab due to its high permittivity, as in an inverted strip waveguide [7]. The TE mode (E_z, H_x, H_y) in a two-dimensional structure (Fig. 1) is sensitive to the bias magnetic field [8]. We will consider the TE mode propagating in the y direction, possessing no variation in the z direction, and having the time dependence $\exp(-j\omega t)$. According to the perturbation method with multiple space scales [4], the sinusoidal function $h(y)$ is given by

$$x = h(y) = h(1 + \delta\eta \cos Ky), \qquad K = 2\pi/\Lambda \tag{1}$$

where δ is the formal expansion parameter, η is the modulation index, and Λ is the periodicity of the corrugation. The permeability tensor $\tilde{\mu}$ of the ferrite slab is given by

$$\tilde{\mu} = \begin{pmatrix} \mu & -j\kappa & 0 \\ j\kappa & \mu & 0 \\ 0 & 0 & 1 \end{pmatrix}, \qquad \mu = 1 + \frac{\omega_0\omega_m}{\omega_0^2 - \omega^2}, \quad \omega_0 = \gamma\mu_0 H_0,$$
$$\kappa = \frac{\omega\omega_m}{\omega_0^2 - \omega^2} \tag{2}$$
$$\omega_m = \gamma\mu_0 M_s$$

where γ, $\mu_0 M_s$, and $\mu_0 H_0$ are the gyromagnetic ratio, the saturation magnetization, and the bias magnetic field, respectively. The phasor amplitude of the electric field E_z satisfies the differential equation

$$\left(\frac{\partial^2}{\partial x^2} + \frac{\partial^2}{\partial y^2} + \epsilon_r\mu_r k^2\right) E_{zr} = 0, \qquad r = a, f, d. \tag{3}$$

0018-9480/88/0300-0568$01.00 ©1988 IEEE

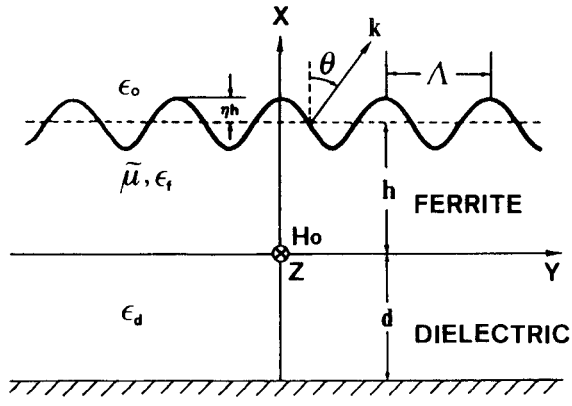

Fig. 1. Analytical model of the corrugated ferrite dielectric slab structure.

We shall identify the quantities corresponding to each layer by index r; that is, the air $(x > h)$ by a, the ferrite slab $(h > x > 0)$ by f, and the dielectric slab $(0 > x > -d)$ by d, respectively. H_x and H_y are expressed in terms of E_z as

$$H_{xr} = \frac{1}{j\omega_0\mu_0\mu_r}\left(\frac{\partial}{\partial y} - j\kappa_r\frac{\partial}{\partial x}\right)E_{zr}, \qquad r = a, f, d \quad (4)$$

$$H_{yr} = \frac{-1}{j\omega_0\mu_0\mu_r}\left(\frac{\partial}{\partial x} + j\kappa_r\frac{\partial}{\partial y}\right)E_{zr}, \qquad r = a, f, d \quad (5)$$

where

$$\mu_f = (\mu^2 - \kappa^2)/\mu, \qquad \kappa_f = \kappa/\mu, \qquad k = \omega_0\sqrt{\epsilon_0\mu_0}\,.$$

In the above equations, k is the wavenumber in free space and ϵ_r is the relative permittivity of each layer. For the air and the dielectric slab, $\mu_r = 1$ and $\kappa_r = 0$ are assumed.

We consider the perturbation up to δ^2. The chain rule is applied as [4]

$$\frac{\partial}{\partial y} = \frac{\partial}{\partial y_0} + \delta^2\frac{\partial}{\partial y_2} \quad (6)$$

and the expansion of the fields is as follows:

$$\Phi(x, y) = \Phi_0(x, y_0, y_2) + \delta\Phi_1(x, y_0, y_2) + \delta^2\Phi_2(x, y_0, y_2), \qquad \Phi = E_z, H_x, H_y. \quad (7)$$

Substituting (6) and (7) into (3) and equating the coefficients of equal power of δ, we get the following differential equations for each order δ^n:

$$o(\delta^n): \left(\frac{\partial^2}{\partial x^2} + \frac{\partial^2}{\partial y_0^2} + \epsilon_r\mu_r k^2\right)E_{zrn} = 0, \qquad n = 0,1;\ r = a, f, d \quad (8)$$

$$o(\delta^2): \left(\frac{\partial^2}{\partial x^2} + \frac{\partial^2}{\partial y_0^2} + \epsilon_r\mu_r k^2\right)E_{zr2} = -2\frac{\partial^2 E_{zr0}}{\partial y_0 \partial y_2}, \qquad r = a, f, d. \quad (9)$$

For simplicity, we will replace the electric field E_{zrn} by E_{rn}, and H_x and H_y by H_{xr} and H_{yr} for each layer.

The boundary conditions are that E_z and H_y must be continuous at $x = 0$, $E_z = 0$ at $x = -d$. For each order δ^n, these become

$$o(\delta^n): E_{fn} = E_{dn}, \qquad n = 0,1,2 \quad (10)$$

$$\frac{1}{\mu_f}\left(\frac{\partial}{\partial x} + j\kappa_f\frac{\partial}{\partial y_0}\right)E_{fn} = \frac{\partial E_{dn}}{\partial x}, \qquad n = 0,1 \quad (11)$$

$$o(\delta^2): \frac{1}{\mu_f}\left[\frac{\partial E_{f2}}{\partial x} + j\kappa_f\left(\frac{\partial E_{f2}}{\partial y_0} + \frac{\partial E_{f0}}{\partial y_2}\right)\right] = \frac{\partial E_{d2}}{\partial x} \quad (12)$$

at $x = 0$, and

$$o(\delta^n): E_{dn} = 0, \qquad n = 0,1,2 \quad (13)$$

at $x = -d$. From the continuity of the tangential electric and magnetic fields at $x = h(y)$, one finds that

$$E_a = E_f \quad (14)$$

$$H_{ya} + \frac{dx}{dy}H_{xa} = H_{yf} + \frac{dx}{dy}H_{xf}. \quad (15)$$

Substituting (4) and (5) into (15), expanding E_z in Taylor series about $x = h$, with the help of (1), (6), and (7), we obtain two sets of equivalent boundary conditions at $x = h$ as follows:

$$o(\delta^0): E_{r0},\ \frac{1}{\mu_r}\left(\frac{\partial}{\partial x} + j\kappa_r\frac{\partial}{\partial y_0}\right)E_{r0}: \text{ continuous, } r = a, f \quad (16)$$

$$o(\delta^1): E_{r1} + h\eta\cos Ky\frac{\partial E_{r0}}{\partial x}, \quad (17a)$$

$$\frac{1}{\mu_r}\left[\left(\frac{\partial}{\partial x} + j\kappa_r\frac{\partial}{\partial y_0}\right)E_{r1} + h\eta\left(\frac{\partial}{\partial x} + j\kappa_r\frac{\partial}{\partial y_0}\right)\cdot\left(\cos Ky\frac{\partial E_{r0}}{\partial x}\right) + h\eta K\sin Ky\cdot\left(\frac{\partial}{\partial y_0} - j\kappa_r\frac{\partial}{\partial x}\right)E_{r0}\right]: \text{ continuous, } r = a, f \quad (17b)$$

$$o(\delta^2): E_{r2} + h\eta\cos Ky\frac{\partial E_{r1}}{\partial x} + \frac{1}{2}(h\eta\cos Ky)^2\frac{\partial^2 E_{r0}}{\partial x^2}, \quad (18a)$$

$$\frac{1}{\mu_r}\left[\frac{\partial E_{r2}}{\partial x} + j\kappa_r\left(\frac{\partial E_{r2}}{\partial y_0} + \frac{\partial E_{r0}}{\partial y_2}\right) + h\eta\left(\frac{\partial}{\partial x} + j\kappa_r\frac{\partial}{\partial y_0}\right)\left(\cos Ky\frac{\partial E_{r1}}{\partial x}\right) + h\eta K\sin Ky\left(\frac{\partial}{\partial y_0} - j\kappa_r\frac{\partial}{\partial x}\right)E_{r1} + \frac{1}{2}h^2\eta^2\left(\frac{\partial}{\partial x} + j\kappa_r\frac{\partial}{\partial y_0}\right)\left(\cos^2 Ky\frac{\partial^2 E_{r0}}{\partial x^2}\right) + h^2\eta^2 K\sin Ky\left(\frac{\partial}{\partial y_0} - j\kappa_r\frac{\partial}{\partial x}\right)\cdot\left(\cos Ky\frac{\partial E_{r0}}{\partial x}\right)\right]: \text{ continuous, } r = a, f. \quad (18b)$$

B. Zero-Order Fields

The zero-order field E_{z0} is referred to as the guided wave [4]. From the wave equation (8), we express the zero-order fields E_{z0} in the waveguide without corrugation as

$$E_{a0} = N_g A_0 e^{-k_1(x-h)} e^{j\beta y_0}, \qquad \infty > x > h \tag{19}$$

$$E_{f0} = N_g \left(B_0 \frac{\cos k_2 x}{\cos k_2 h} + C_0 \frac{\sin k_2 x}{\sin k_2 h} \right) e^{j\beta y_0}, \qquad h > x > 0 \tag{20}$$

$$E_{d0} = N_g D_0 \frac{\sinh\left[k_3(x+d)\right]}{\sinh(k_3 d)} e^{j\beta y_0}, \qquad 0 > x > -d \tag{21}$$

where

$$k_1^2 = \beta^2 - k^2, \qquad k_2^2 = \epsilon_f \mu_f k^2 - \beta^2, \qquad k_3^2 = \beta^2 - \epsilon_d k^2. \tag{22}$$

By applying the boundary conditions (10), (11), and (16) for the zero-order fields (19)–(21), we obtain that

$$[\Xi][F_0] = 0 \tag{23}$$

where $[F_0]$ is a 4×1 matrix with unknown constants A_0, B_0, C_0, and D_0, and the elements of the 4×4 matrix $[\Xi]$ are given by

$$\begin{aligned}
&\xi_{14} = \xi_{24} = \xi_{31} = \xi_{33} = \xi_{41} = 0 \\
&\xi_{11} = -\xi_{12} = -\xi_{13} = \xi_{32} = 1, \qquad \xi_{21} = \mu_f k_1 \\
&\xi_{22} = k_2 \tan k_2 h + \kappa_f \beta, \qquad \xi_{23} = \kappa_f \beta - k_2 \cot k_2 h \\
&\xi_{34} = -\cos k_2 h, \qquad \xi_{42} = -\kappa_f \beta, \qquad \xi_{43} = k_2 \cot k_2 h \\
&\xi_{44} = -\mu_f k_3 \cos k_2 h \coth(k_3 d).
\end{aligned} \tag{24}$$

With the help of (23), the unknown constants in (20) and (21) can be replaced by A_0 in (19) as follows:

$$B_0 = \frac{1}{k_2} \cos k_2 h \left(R \sin k_2 h + k_2 \cos k_2 h \right) A_0 \tag{25a}$$

$$C_0 = \frac{1}{k_2} \sin k_2 h \left(k_2 \sin k_2 h - R \cos k_2 h \right) A_0 \tag{25b}$$

$$D_0 = \frac{B_0}{\cos k_2 h} \tag{25c}$$

where

$$R = \mu_f k_1 - \kappa_f \beta.$$

From the condition of the nontrivial solution of (23), $\det[\Xi] = 0$, we obtain the zero-order dispersion relation

$$\frac{1}{\mu_f}\left[k_2^2 - \kappa_f \beta\left(\mu_f k_1 - \kappa_f \beta\right)\right] \tan k_2 h \tanh(k_3 d) - k_2 k_3 + k_3\left(\kappa_f \beta - \mu_f k_1\right) \tan k_2 h - k_1 k_2 \tanh(k_3 d) = 0. \tag{26}$$

In (19)–(21), the normalization constant N_g is chosen in such a way that the power P_{gy} carried by the guided wave in the y direction over a unit width in the z direction is obtained as $P_{gy} = |A_0|^2$. By utilizing the relation given in (25a)–(25c), N_g can be derived as

$$N_g = \left[\frac{4\omega\mu_0 \mu_f k_1 k_2^3 k_3}{U} \right]^{1/2} \tag{27}$$

where

$$\begin{aligned}
U &= \mu_f \beta k_2^3 k_3 + k_1 \cos^2 k_2 h \left(k_3 V + \mu_f \beta k_2 S^2 W \right) \\
V &= \beta k_2 h (S^2 + T^2) + k_2 \left(\beta R - \kappa_f k_2^2 \right) / \\
&\quad \cos^2 k_2 h + S\left(\kappa_f k_2 S - \beta T \right) \\
W &= \cot h (k_3 d) - k_3 d / \sinh^2 (k_3 d) \\
S &= k_2 + R \tan k_2 h, \qquad T = R - k_2 \tan k_2 h.
\end{aligned}$$

C. First-Order Fields

The perturbed first-order fields are caused by the originally excited wave due to a corrugation. From the boundary conditions (17a) and (17b), we can find that the propagation constants of the first-order field are $\beta_{11} = \beta - K$ and $\beta_{12} = \beta + K$ for space harmonics $m = \pm 1$. The first-order solution of E_z, including the amplitudes of the incident wave A_i and of the radiated wave A_r, can be expressed as a combination of two scattered Floquet modes β_{11} and β_{12} for each region:

$$\begin{aligned}
E_{a1} &= N_r \left[A_i e^{-j\alpha_1(x-h)} + A_r e^{j\alpha_1(x-h)} \right] e^{j\beta_{11} y_0} \\
&\quad + A_1 e^{-\alpha_2(x-h)} e^{j\beta_{12} y_0}, \qquad \infty > x > h
\end{aligned} \tag{28}$$

$$\begin{aligned}
E_{f1} &= \left(B_{11} \frac{\cos \alpha_3 x}{\cos \alpha_3 h} + C_{11} \frac{\sin \alpha_3 x}{\sin \alpha_3 h} \right) e^{j\beta_{11} y_0} \\
&\quad + \left(B_{12} \frac{\cos \alpha_4 x}{\cos \alpha_4 h} + C_{12} \frac{\sin \alpha_4 x}{\sin \alpha_4 h} \right) e^{j\beta_{12} y_0}, \qquad h > x > 0
\end{aligned} \tag{29}$$

$$E_{d1} = D_{11} \frac{\sin \alpha_5 (x+d)}{\sin \alpha_5 d} e^{j\beta_{11} y_0} + D_{12} \frac{\sin \alpha_6 (x+d)}{\sin \alpha_6 d} e^{j\beta_{12} y_0}, \qquad 0 > x > -d \tag{30}$$

where

$$\begin{aligned}
&\alpha_1^2 = k^2 - \beta_{11}^2, \qquad \alpha_2^2 = \beta_{12}^2 - k^2, \qquad \alpha_3^2 = \mu_f \epsilon_f k^2 - \beta_{11}^2 \\
&\alpha_4^2 = \mu_f \epsilon_f k^2 - \beta_{12}^2, \qquad \alpha_5^2 = \epsilon_d k^2 - \beta_{11}^2, \qquad \alpha_6^2 = \epsilon_d k^2 - \beta_{12}^2.
\end{aligned} \tag{31}$$

In (28), the normalization constant N_r is chosen in such a way that the $-x$ and $+x$ components of the Poynting vectors P_{-x} and P_{+x} associated with the incident and radiated waves become $|A_i|^2$ and $|A_r|^2$, respectively. N_r is deduced as

$$N_r = (2\omega\mu_0/\alpha_1)^{1/2}. \tag{32}$$

By applying the boundary conditions of the first-order fields, that is (10), (11), (17a), and (17b), we can, with the help of (25a)–(25c), express the unknown constants of the

first-order fields (28)–(30) as

$$B_{11} = (M_1/M)\left[\frac{1}{2}h\eta(P_1 + j\alpha_1\mu_f P)N_g A_0 - 2j\alpha_1\mu_f N_r A_t\right] \tag{33a}$$

$$C_{11} = (M_2/M)\left[\frac{1}{2}h\eta(P_1 + j\alpha_1\mu_f P)N_g A_0 - 2j\alpha_1\mu_f N_r A_t\right] \tag{33b}$$

$$D_{11} = B_{11}/\cos\alpha_3 h \tag{33c}$$

and

$$A_1 = \frac{1}{2}h\eta\left[P + (P_2 - \alpha_2\mu_f P)(N_1 + N_2)/N\right]N_g A_0 \tag{34a}$$

$$B_{12} = \frac{1}{2}h\eta\left[(P_2 - \alpha_2\mu_f P)N_1/N\right]N_g A_0 \tag{34b}$$

$$C_{12} = \frac{1}{2}h\eta\left[(P_2 - \alpha_2\mu_f P)N_2/N\right]N_g A_0 \tag{34c}$$

$$D_{12} = B_{12}/\cos\alpha_4 h \tag{34d}$$

where

$$P = k_1 - R$$

$$P_1 = (\mu_f k_1^2 + k_2^2) + \beta K(1-\mu_f) - \kappa_f R(\beta - 2K)$$

$$P_2 = (\mu_f k_1^2 + k_2^2) - \beta K(1-\mu_f) - \kappa_f R(\beta + 2K)$$

$$M = (\alpha_3\cot\alpha_3 h - \kappa_f\beta_{11} - j\alpha_1\mu_f)M_2 - (\alpha_3\tan\alpha_3 h + \kappa_f\beta_{11} + j\alpha_1\mu_f)M_1$$

$$N = (\alpha_4\cot\alpha_4 h - \kappa_f\beta_{12} + \alpha_2\mu_f)N_2 - (\alpha_4\tan\alpha_4 h + \kappa_f\beta_{12} - \alpha_2\mu_f)N_1$$

$$M_1 = \alpha_3\cot\alpha_3 h, \qquad M_2 = \mu_f\alpha_5\cot\alpha_5 d + \kappa_f\beta_{11}$$

$$N_1 = \alpha_4\cot\alpha_4 h, \qquad N_2 = \mu_f\alpha_6\cot\alpha_6 d + \kappa_f\beta_{12}.$$

From the boundary conditions of the first-order fields, a relation between the amplitudes of the principal guided wave A_0, the incident wave A_t, and the radiated wave A_r can be derived as

$$A_r = C_{rg}A_0 + C_{rr}A_t \tag{35}$$

where

$$C_{rg} = \frac{1}{2}h\eta\left[P + (P_1 + j\alpha_1\mu_f P)(M_1 + M_2)/M\right]N_g/N_r \tag{36}$$

$$C_{rr} = -\frac{M^*}{M}. \tag{37}$$

In (36), C_{rg} and C_{rr} are the coupling and reflection coefficients, respectively, and M^* in (37) is the complex conjugate of M.

D. Second-Order Fields

The analysis of the second-order fields clarifies how the guided mode amplitude and phase change in the corrugated waveguide. Here, we assume particular solutions for E_{r2} in the form

$$E_{a2} = \phi_a(x)e^{j\beta y_0}, \qquad \infty > x > h \tag{38}$$

$$E_{f2} = \phi_f(x)e^{j\beta y_0}, \qquad h > x > 0 \tag{39}$$

$$E_{d2} = \phi_d(x)e^{j\beta y_0}, \qquad 0 > x > -d. \tag{40}$$

Substituting (38)–(40) and (19)–(21) into (9), we obtain the following differential equations for $\phi_r(x)$:

$$\left(\frac{\partial^2}{\partial x^2} - k_1^2\right)\phi_a(x) = -2j\beta N_g\frac{\partial A_0}{\partial y_2}e^{-k_1(x-h)} \tag{41}$$

$$\left(\frac{\partial^2}{\partial x^2} + k_2^2\right)\phi_f(x) = -2j\beta N_g\left(\frac{\partial B_0}{\partial y_2}\frac{\cos k_2 x}{\cos k_2 h} + \frac{\partial C_0}{\partial y_2}\frac{\sin k_2 x}{\sin k_2 h}\right) \tag{42}$$

$$\left(\frac{\partial^2}{\partial x^2} - k_3^2\right)\phi_d(x) = -2j\beta N_g\frac{\partial D_0}{\partial y_2}\frac{\sinh[k_3(x+d)]}{\sinh(k_3 d)}. \tag{43}$$

Solving (41)–(43), we can obtain the solutions

$$\phi_a(x) = \frac{j\beta}{k_1}N_g\frac{\partial A_0}{\partial y_2}xe^{-k_1(x-h)} + A_2e^{-k_1(x-h)} \tag{44}$$

$$\phi_f(x) = -\frac{j\beta}{k_2}N_g x\left(\frac{\partial B_0}{\partial y_2}\frac{\sin k_2 x}{\cos k_2 h} - \frac{\partial C_0}{\partial y_2}\frac{\cos k_2 x}{\sin k_2 h}\right) + B_2\frac{\cos k_2 x}{\cos k_2 h} + C_2\frac{\sin k_2 x}{\sin k_2 h} \tag{45}$$

$$\phi_d(x) = -\frac{j\beta}{k_3}N_g(x+d)\frac{\cosh[k_3(x+d)]}{\sinh(k_3 d)} + D_2\frac{\sinh[k_3(x+d)]}{\sinh(k_3 d)}. \tag{46}$$

By applying the boundary conditions of the second-order fields at $x = h$ and $x = 0$, that is, (10), (12), (18a), and (18b) for the Floquet mode $\exp(j\beta y_0)$, the following matrix equation is obtained:

$$[\Xi][F_2] = [U] \tag{47}$$

where $[F_2]$ is a 4×1 matrix with unknown constants of the second-order fields A_2, B_2, C_2, and D_2 of (44)–(46). The elements of the 4×1 matrix $[U]$ of (47) are given as

$$U_1 = j\beta h\left(\frac{1}{k_1} + \frac{R}{k_2^2}\right)N_g\frac{\partial A_0}{\partial y_2} - \left(\frac{1}{2}h\eta\right)^2(k_1^2 + k_2^2)N_g A_0 + \frac{1}{2}h\eta[j\alpha_1 N_r(A_t - A_r) + \alpha_2 A_1] - \frac{1}{2}h\eta[\alpha_3(B_{11}\tan\alpha_3 h - C_{11}\cot\alpha_3 h) + \alpha_4(B_{12}\tan\alpha_4 h - C_{12}\cot\alpha_4 h)] \tag{48a}$$

$$U_2 = -j\beta\left[\mu_f\left(\frac{1}{k_1}-h\right)+\frac{R}{k_2^2}(1-\kappa_f\beta h)+h-\frac{\kappa_f}{\beta}\right]N_g\frac{\partial A_0}{\partial y_2}$$
$$+\left(\frac{1}{2}h\eta\right)^2\left[\mu_f k_1\left(k_1^2+k_2^2\right)-2\kappa_f\beta K^2\right]N_g A_0$$
$$+\frac{1}{2}h\eta\left[\mu_f N_r(\alpha_1^2-\beta_{11}K)(A_i+A_r)\right.$$
$$+(\beta_{11}K-\alpha_3^2)(B_{11}+C_{11})$$
$$\left.+\kappa_f\alpha_3\beta_{12}(B_{11}\tan\alpha_3 h-C_{11}\cot\alpha_3 h)\right]$$
$$+\frac{1}{2}h\eta\left[\mu_f(\beta_{12}K-\alpha_2^2)A_1-(\beta_{12}K+\alpha_4^2)(B_{12}+C_{12})\right.$$
$$\left.+\kappa_f\alpha_4\beta_{11}(B_{12}\tan\alpha_4 h-C_{12}\cot\alpha_4 h)\right] \quad (48b)$$

$$U_3 = -\frac{j\beta d}{k_3^2}\coth(k_3 d)N_g\frac{\partial B_0}{\partial y_2} \quad (48c)$$

$$U_4 = -j\beta\left[\frac{\kappa_f}{\beta}+\mu_f\left\{\frac{1}{k_3}\coth(k_3 d)+d\right\}\right]N_g\frac{\partial B_0}{\partial y_2}$$
$$-\frac{j\beta}{k_2}\cot k_2 h N_g\frac{\partial C_0}{\partial y_2}. \quad (48d)$$

In (47), the 4×4 matrix $[\Xi]$ is the same as in (23). Assuming a solution of (47), we may select the following relation as one of the solvability conditions:

$$\Xi_{11}U_1+\Xi_{21}U_2+\Xi_{31}U_3+\Xi_{41}U_4=0 \quad (49)$$

where Ξ_{n1}, $n=1$ to 4, are the cofactor for each element of the first row of $\det[\Xi]$. These can be obtained as

$$\Xi_{11}=\frac{\mu_f k_1 k_2^2}{S\sin k_2 h} \quad (50a)$$

$$\Xi_{21}=\frac{k_2^2}{S\sin k_2 h} \quad (50b)$$

$$\Xi_{31}=-\frac{1}{\sin k_2 h}\mu_f k_2 k_3\coth(k_3 d) \quad (50c)$$

$$\Xi_{41}=\frac{k_2}{\sin k_2 h}. \quad (50d)$$

In (48a)–(48d) and (50a)–(50d), R and S are the same values as those defined in (25) and (27), respectively. Substituting (48a)–(48d) and (50a)–(50d) into (49), eliminating the unknown constants A_2, B_2, C_2, and D_2 from (49), and with the help of (25a)–(25c) and (33)–(35), we get an amplitude transport equation as

$$\frac{\partial A_0}{\partial y_2}=C_{gg}A_0+C_{gr}A_i. \quad (51)$$

In the above equation, C_{gg} and C_{gr} are defined as

$$C_{gg}=\frac{j}{U}\left(\frac{1}{2}h\eta\right)^2 k_1 k_2^3 k_3 Q_1 \quad (52)$$

$$C_{gr}=\frac{1}{MUN_g}(h\eta)\mu_f\alpha_1 k_1 k_2^3 k_3 Q_2 N_r \quad (53)$$

where

$$Q_1=2\kappa_f\beta K^2+\mu_f P\left[\alpha_2^2-\alpha_1^2-2K^2+k_1(j\alpha_1-\alpha_2)\right]$$
$$+(P_1+j\alpha_1\mu_f P)G_1/M+(P_2-\alpha_2\mu_f P)G_2/N$$
$$Q_2=(P+\kappa_f K)M+(M_1+M_2)\left[(P_1+j\alpha_1\mu_f P)\right.$$
$$\left.+\kappa_f K(\kappa_f\beta_{11}-R+j\alpha_1\mu_f)\right]$$
$$G_1=(M_1+M_2)\left[\alpha_3-\mu_f\alpha_1^2-\beta_{11}K(1-\mu_f)+j\alpha_1\mu_f k_1\right]$$
$$+\alpha_3(R-\kappa_f K)(M_1\tan\alpha_3 h-M_2\cot\alpha_3 h)$$
$$G_2=(N_1+N_2)\left[\alpha_4^2+\mu_f\alpha_2^2+\beta_{12}K(1-\mu_f)-\alpha_2\mu_f k_1\right]$$
$$+\alpha_4(R+\kappa_f K)(N_1\tan\alpha_4 h-N_2\cot\alpha_4 h).$$

Other quantities in (52) and (53) are the same parameters as those given in the previous sections. In (51), C_{gg} is the extinction coefficient and the real part C_{ggr} of C_{gg} is defined as the leakage coefficient [4]–[6].

Since the operation of a transmitting antenna is based on the scattering of a guided wave into a radiated wave due to the presence of corrugation, the incident wave amplitude A_i is assumed to be zero. Setting $A_i=0$ in (51), the radiation efficiency Q_0 of the leaky wave can be deduced as [4]

$$Q_0=-\frac{|C_{rg}|^2}{2C_{ggr}}(1-e^{2C_{ggr}L}) \quad (54)$$

where L is the corrugation length. The radiation angle θ is given by

$$\theta=\arcsin\left(\frac{\beta-K+C_{ggi}}{k}\right) \quad (55)$$

where C_{ggi} is the imaginary part of C_{gg}. Since θ is a function of the bias magnetic field $\mu_0 H_0$, θ can be controlled by altering $\mu_0 H_0$.

III. Numerical Calculation

In order to clarify the radiation characteristics of the waveguide structure of Fig. 1, the amplitude transport equations (35) and (51) are solved numerically. The material parameters of the ferrite slab are assumed to be $\mu_0 M_s=1730$ G, $h=0.925$ mm, $\epsilon_f=15.6$, $\eta=0.081$, $\Lambda=2$ mm, and $L=110$ mm (number of periods of the corrugation $N=55$). For the dielectric slab, $d=3.4$ mm and $\epsilon_d=2.1$.

The dispersion diagram is obtained numerically from the zero-order dispersion relation of (26) at a fixed bias magnetic field 0.8 T and is shown in Fig. 2. In the closed area between the dotted lines $\beta_1=k\sqrt{\epsilon_d}$ and $\beta_2=k\sqrt{\epsilon_f\mu_f}$ above 25 GHz in the diagram, the electromagnetic fields distribute hyperbolic functionally in the dielectric slab and sinusoidally in the ferrite slab regions. In the frequency range 40 to 50 GHz, both TE_0 and TE_1 modes can propagate, but the TE_0 mode only lies in the radiation region, $K-k<\beta<K+k$, which is defined with (55) by neglecting the small value of C_{ggi}, and is shown within a triangular region enclosed by the chained lines in the figure. An abrupt change of the propagation constant of

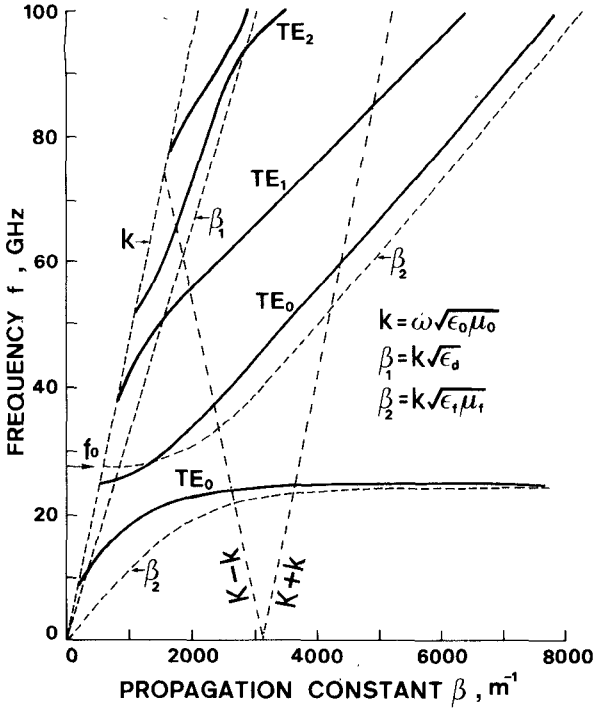

Fig. 2. Dispersion diagram for TE mode in a layered ferrite dielectric slab structure at a fixed bias magnetic field 0.8 T.

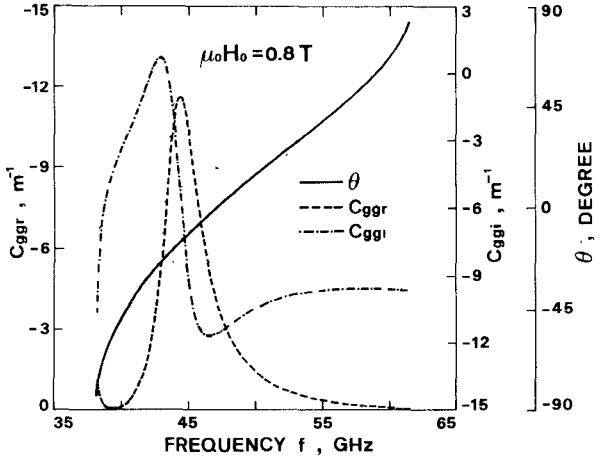

Fig. 3. Variation of the real and imaginary parts of the extinction coefficient and the radiation angle of the fundamental TE mode as a function of the frequency.

the TE_0 mode is observed near the gyromagnetic resonance frequency $f_0 = (\omega_0 + \omega_m)/(2\pi)$ ($f_0 = 27.2$ GHz for $\mu_0 H_0 = 0.8$ T).

The extinction coefficient $C_{ggr} + jC_{ggi}$ and the radiation angle θ are estimated numerically from (52) and (55) as a function of the frequency, as shown in Fig. 3. It is noted that both C_{ggr} and C_{ggi} depend strongly on the frequency and have maximum values near 45 GHz. While θ varies monotonically with increasing frequency, and the rate of its change ($d\theta/df$) is larger in the lower frequency range than in the higher one. Since the leakage coefficient C_{ggr} also depends upon the thicknesses h and d, the periodicity of the corrugation Λ, the saturation magnetization of

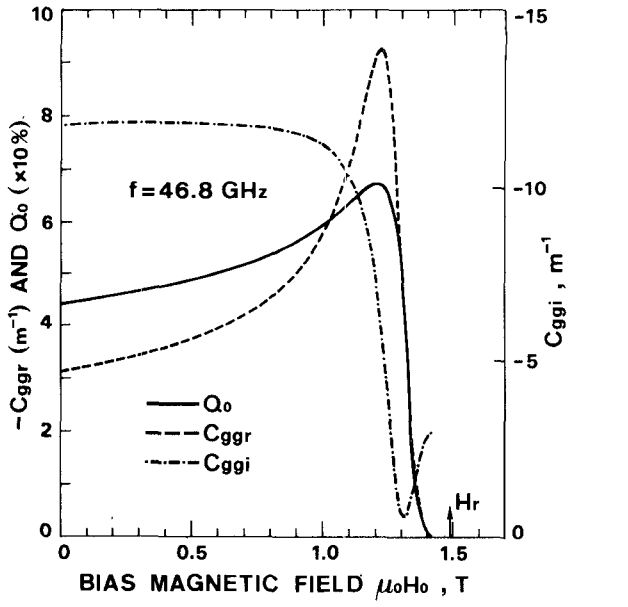

Fig. 4. Variation of the real and imaginary parts of the extinction coefficient and the radiation efficiency as a function of the bias magnetic field at a fixed frequency 46.8 GHz.

ferrite $\mu_0 M_s$, and the permittivities ϵ_f and ϵ_d, with the exception of f and $\mu_0 H_0$, we may expect that the radiation characteristics can be improved by carefully selecting those structural and physical parameters.

The radiation efficiency Q_0 defined by (54) and C_{gg} are shown in Fig. 4 as a function of the bias magnetic field. It is noted that Q_0 increases with increasing H_0 and has a maximum value of 67.4 percent. But it approaches zero near the gyromagnetic resonance field $\mu_0 H_r = (\omega - \omega_m)/\gamma$ ($\mu_0 H_r = 1.498$ T as $f = 46.8$ GHz).

IV. Experimental Results

Experiments are performed in the frequency range from 40 to 50 GHz. The upper surface of a polycrystalline yttrium iron garnet (YIG) slab with dimensions of $1.0 \times 15.0 \times 150.0$ $(\text{mm})^3$ has an array of rectangular grooves. The width, depth, corrugation spacing, and number of periods of the corrugation are 1.0 mm, 150 μm ($h\eta = 75$ μm), $\Lambda = 2$ mm, and $N = 55$, respectively. The corrugated YIG slab is supported by a Teflon slab bonded to a copper plane by low-loss wax as shown in Fig. 1. The width and the length of Teflon slab are 11.65 mm and 150.0 mm, respectively.

In order to excite the TE mode in the corrugated structure, the upper surface of ferrite slab is held parallel to the electric field of the TE_{10} mode at the output end of the rectangular metal waveguide. Both ends of the layered slab are tapered and one side is coated with a carbon absorber to avoid the unwanted reflection of the waves. The corrugated structure is magnetized in a direction parallel to its plane by an electromagnet. The radiated signal is detected through a standard horn at a distance of 106.5 cm from the center of the corrugated ferrite slab. Here, detailed explanations of the experimental setup used in these experi-

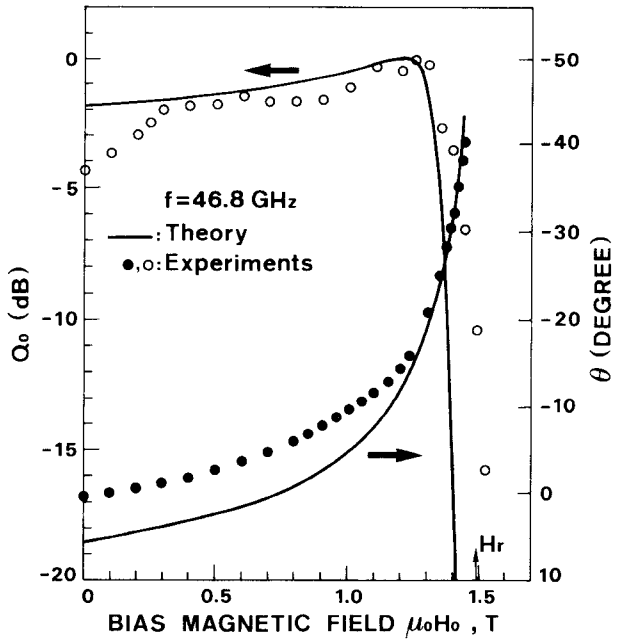

Fig. 5. Theory and experiment for the main bean direction and the radiation efficiency (amplitude of the main beam) versus the bias magnetic field at a fixed frequency 46.8 GHz.

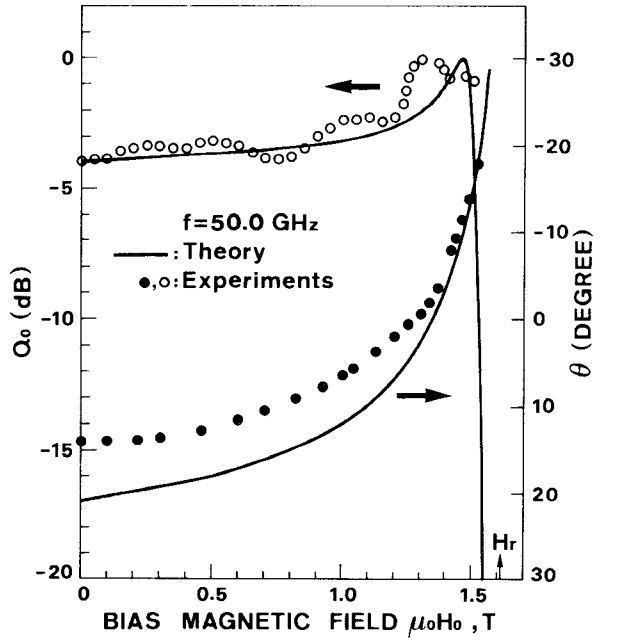

Fig. 6. Theory and experiment for the main beam direction and the radiation efficiency (amplitude of the main beam) versus the bias magnetic field at a fixed frequency 50.0 GHz.

ments are omitted because they have been given in [2] and [3].

Figs. 5 and 6 show the measured radiation angle and the amplitude of the main beam as a function of the bias magnetic field for different frequencies 46.8 and 50.0 GHz, respectively. The solid lines of the radiation angle θ are obtained from (55). By increasing the bias magnetic field, a continuous scanning of the main beam up to $-40.5°$ is observed in Fig. 5. The slope scanning rate $\Delta\theta/\Delta(\mu_0 H_0)$, increases rapidly as the magnetic field approaches the gyromagnetic resonance field $\mu_0 H_r \approx 1.5$ T. The maximum scanning rate can be estimated with $1°/200$ G. Similar scanning characteristics of the main beam are obtained at the frequency 50.0 GHz, as shown in Fig. 6.

The relative values of the main beam amplitude A_r' are measured by using a dc voltmeter. At the operating frequency of 46.8 GHz in Fig. 5, the maximum value of A_r', $(A_r')_{\max}$, found experimentally is 19 mV, whereas at 50 GHz in Fig. 6 it decreases to 12 mV, as predicted by the theoretical results on C_{ggr} (Fig. 3). Because it is difficult to compare directly the experimental data on A_r' with the theoretical results on Q_0, A_r' is transformed into decibel form as $10\log[A_r'/(A_r')_{\max}]$, which may be considered as an approximation of the radiation efficiency Q_0. Here, we used a square law detector.

The solid lines of the radiation efficiency in the figures are estimated numerically with (54). In Fig. 5, Q_0 is found both theoretically and experimentally to decrease rapidly in the vicinity of the gyromagnetic resonance field.

Through these experiments it is concluded that the experimental data agree well with the theoretical predictions within the experimental accuracy.

V. Conclusion

The leaky wave phenomena of the corrugated ferrite slab supported by a grounded dielectric slab are analyzed using the perturbation method with multiple space scales. The amplitude transport equations which give the relation between the guided and the radiated waves are derived. The radiation efficiency and the angle of radiation are estimated numerically by solving the amplitude transport equations.

Experiments were performed in the frequency range 40 to 50 GHz using a corrugated polycrystalline YIG slab fixed on a grounded Teflon slab. The main beam direction and the amplitude of the leaky wave were measured as a function of the bias magnetic field for two different frequencies 46.8 and 50.0 GHz. The main beam direction could be steered continuously by changing the bias magnetic field. The maximum scanning rate was about $1°/200$ G. These experimental results are in fairly good agreement with the theory.

The corrugated ferrite dielectric slab waveguide proposed in this paper may be useful for the application of the electrically scannable leaky wave antenna in the millimeter-wave frequency. If we select carefully the structural parameters of the system, we may develop a mm-wave antenna having a high resolution and a radiation beam whose direction can be controlled by changing the bias magnetic field.

References

[1] P. Bhartia and I. J. Bahl, *Millimeter Wave Engineering and Applications* New York: Wiley, 1984, pp. 307–598.

[2] T. Ohira, M. Tsutsumi, and N. Kumagai, "Radiation of millimeter waves from a grooved ferrite image line," *Proc. IEEE*, vol. 70, pp. 682–683, June 1982.

[3] H. Maheri, M. Tsutsumi, and N. Kumagai, "Magnetically scannable leaky wave antenna using the layered corrugated ferrite slab structure," *IEEE Trans. Antennas Propagat.*, to be published.
[4] W. S. Park and S. R. Seshadri, "Theory of the grating coupler for a grounded-dielectric-slab waveguide," *Proc. Inst. Elec. Eng.*, vol. 132, pt. H, pp. 149–156, June 1985.
[5] W. S. Park and S. R. Seshadri, "Reradiation from a grating coupler for a grounded dielectric slab waveguide," *Proc. Inst. Elec. Eng.*, vol. 133, pt. H, pp. 10–17, Feb. 1986.
[6] M. T. Wlodarczyk and S. R. Seshadri, "Excitation and scattering of guided modes on a helically corrugated dielectric cylinder," *IEEE Trans. Microwave Theory Tech.*, vol. MTT-34, pp. 8–18, Jan. 1986.
[7] T. Itoh, "Inverted strip dielectric waveguide for millimeter-wave integrated circuits," *IEEE Trans. Microwave Theory Tech.*, vol. MTT-24, pp. 821–827, Nov. 1976.
[8] T. J. Gerson and J. S. Nadan, "Surface electromagnetic modes of ferrite slab," *IEEE Trans. Microwave Theory Tech.*, vol. MTT-22, pp. 757–762, Aug. 1974.

✠

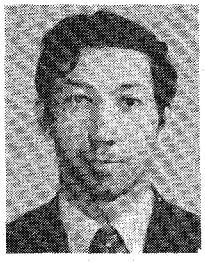

Sidick Erkin was born in Xin Jiang, China, April 25, 1958. He received the B.S. degree in electrical engineering from Xin Jiang University, Urumqi, Xin Jiang, China, in February 1983. Since March 1983, he has been a Teaching Assistant in the Physics Department at Xin Jiang University, Urumqi, Xin Jiang, People's Republic of China.

From 1983 to 1984, he was a Visiting Scholar at the Department of Electronic Engineering, Shang Hai Jiao Tung University, Shang Hai, People's Republic of China, where he was interested in electromagnetic theory, microwave theory and technique. Since September 1985, he has been a Guest Researcher with the Department of Communication Engineering, Osaka Electro-Communication University, Neyagawa, Osaka, Japan, where he has been engaged in research work on microwave and millimeter-wave ferrite devices.

Mr. Erkin is a member of the Institute of Electronics, Information and Communication Engineers of Japan.

✠

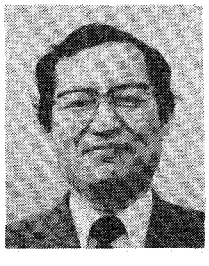

Nion Sock Chang (S'58–M'64) was born in Ursan, Korea, on April 15, 1927. He received the B.S. degree in electrical engineering from Ritsumeikan University, Kyoto, Japan, in 1953, and the M.S. and Ph.D. degrees from Osaka University, Osaka, Japan, in 1958 and 1965, respectively.

In 1966 he joined the Institute of Science and Industrial Research, Osaka University, as a Research Assistant. Since 1981 he has been a Professor at Osaka Electro-Communication University, where he is engaged in propagation studies in dielectric and magnetic layered structures with a sinusoidal corrugation. Recently, he became head of the Institute of Satellite Communication Research at the same university. He is also involved in research on the radio-wave propagation on the earth-space path including XPD measurement.

Dr. Chang is a member of the Institute of Electronics, Information and Communication Engineers of Japan and Japan Society of Applied Physics.

✠

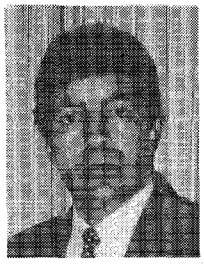

Heshmatollah Maheri was born in Kerman, Iran, on April 21, 1947. He received the Dipl. Ing. degree in communication engineering from the Technical University of Aachen, Federal Republic of Germany, in 1976. His graduate thesis work involved stripline resonators, and studies on the material parameters of polycrystalline ferrites in the *X*- and *K*-band frequency ranges.

From 1976 to 1983 he was a Lecturer in the Department of Electrical Engineering at the Technical College of Kerman, the University of Guilan, and the Kerman University, in Iran. He also served as head of the Electrical Engineering Department in the Technical College of Kerman and the University of Guilan. In April 1984 he continued his graduate studies at Osaka University, Osaka, Japan, as a recipient of a Mombusho Scholarship from the Japanese Government. In March 1987 he received the Ph.D. degree in communication engineering, based on research in millimeter-wave integrated circuits containing ferrites.

Currently, Dr. Maheri is attached to the Research Laboratory of the Antennas and Satellite Communication Department of Mitsubishi Electric Corporation, in Osaka, Japan. His present research interests are mainly in microwave and millimeter-wave antennas and associated measurement techniques.

Dr. Maheri is a member of the Institute of Electronics, Information and Communication Engineers of Japan.

✠

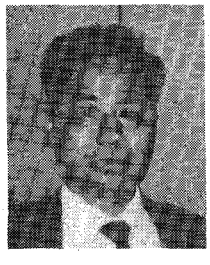

Makoto Tsutsumi (M'71) was born in Tokyo, Japan, on February 25, 1937. He received the B.S. degree in electrical engineering from Ritsumeikan University, Kyoto, in 1961, and the M.S. and Ph.D. degrees in communication engineering from Osaka University, Osaka, Japan, in 1963 and 1971, respectively.

From 1974 to 1983, he was a Lecturer, and since 1984 he has been an Associate Professor of Communication Engineering at Osaka University. His research interests are primarily in microwave and millimeter-wave ferrite devices. He has published 80 technical papers on these topics in various journals.

Dr. Tsutsumi is a member of the Institute of Electronics, Information and Communication Engineers of Japan and the Japan Society of Applied Physics.